

Journal of Biomedical Optics

BiomedicalOptics.SPIEDigitalLibrary.org

Validating tyrosinase homologue *mela* as a photoacoustic reporter gene for imaging *Escherichia coli*

Robert J. Paproski
Yan Li
Quinn Barber
John D. Lewis
Robert E. Campbell
Roger Zemp

Validating tyrosinase homologue *melA* as a photoacoustic reporter gene for imaging *Escherichia coli*

Robert J. Paproski,^{a,b,†} Yan Li,^{c,†} Quinn Barber,^a John D. Lewis,^b Robert E. Campbell,^c and Roger Zemp^{a,*}

^aUniversity of Alberta, Department of Electrical and Computer Engineering, Donadeo Innovation Centre for Engineering, 9211-116 Street, Edmonton, Alberta T6G 1H9, Canada

^bUniversity of Alberta, Department of Oncology, Katz Group Centre, 114 Street & 87 Avenue, Edmonton, Alberta T6G 2E1, Canada

^cUniversity of Alberta, Department of Chemistry, 11227 Saskatchewan Drive, Edmonton, Alberta T6G 2G2, Canada

Abstract. To understand the pathogenic processes for infectious bacteria, appropriate research tools are required for replicating and characterizing infections. Fluorescence and bioluminescence imaging have primarily been used to image infections in animal models, but optical scattering in tissue significantly limits imaging depth and resolution. Photoacoustic imaging, which has improved depth-to-resolution ratio compared to conventional optical imaging, could be useful for visualizing *melA*-expressing bacteria since *melA* is a bacterial tyrosinase homologue which produces melanin. *Escherichia coli*-expressing *melA* was visibly dark in liquid culture. When *melA*-expressing bacteria in tubes were imaged with a VisualSonics Vevo LAZR system, the signal-to-noise ratio of a 9× dilution sample was 55, suggesting that ~20 bacteria cells could be detected with our system. Multispectral (680, 700, 750, 800, 850, and 900 nm) analysis of the photoacoustic signal allowed unmixing of *melA*-expressing bacteria from blood. To compare photoacoustic reporter gene *melA* (using Vevo system) with luminescent and fluorescent reporter gene Nano-lantern (using Bruker Xtreme In-Vivo system), tubes of bacteria expressing *melA* or Nano-lantern were submerged 10 mm in 1% Intralipid, spaced between <1 and 20 mm apart from each other, and imaged with the appropriate imaging modality. Photoacoustic imaging could resolve the two tubes of *melA*-expressing bacteria even when the tubes were less than 1 mm from each other, while bioluminescence and fluorescence imaging could not resolve the two tubes of Nano-lantern-expressing bacteria even when the tubes were spaced 10 mm from each other. After injecting 100- μ L of *melA*-expressing bacteria in the back flank of a chicken embryo, photoacoustic imaging allowed visualization of *melA*-expressing bacteria up to 10-mm deep into the embryo. Photoacoustic signal from *melA* could also be separated from deoxy- and oxy-hemoglobin signal observed within the embryo and chorioallantoic membrane. Our results suggest that *melA* is a useful photoacoustic reporter gene for visualizing bacteria, and further work incorporating photoacoustic reporters into infectious bacterial strains is warranted. © The Authors. Published by SPIE under a Creative Commons Attribution 3.0 Unported License. Distribution or reproduction of this work in whole or in part requires full attribution of the original publication, including its DOI. [DOI: [10.1117/1.JBO.20.10.106008](https://doi.org/10.1117/1.JBO.20.10.106008)]

Keywords: *melA*; photoacoustic imaging; bacteria; reporter gene.

Paper 150353PR received May 29, 2015; accepted for publication Sep. 22, 2015; published online Oct. 21, 2015.

1 Introduction

Visualization of gene expression with reporter genes has greatly increased our understanding of mammalian and bacterial cells.¹⁻⁴ Reporter genes encode proteins that can be detected due to the optical properties of the proteins or the products formed by the proteins. Detection of protein levels allows quantification of gene expression which correlates with promoter activity. Reporter genes are also useful for tracking infection processes by imaging bacteria within infected animals.⁵ Several virulence promoters have been identified, and expressing reporter genes with such promoters can identify anatomical sites that correlate with the expression of key virulent factors.^{6,7}

The *lacZ* gene, which encodes β -galactosidase, was one of the first reporter genes identified and used in microbiology.⁸ β -Galactosidase cleaves X-gal (5-bromo-4-chloro-3-indolyl- β -D-galactopyranoside), producing a dark-blue product that

can be quantified by its strong optical absorption. The enzymatic activity of β -galactosidase allows very sensitive detection of *lacZ* expression, but the requirement of synthetic X-gal complicates its use *in vivo* since X-gal is not naturally present in animals and can cause irritation and inflammation when injected in rodents.⁹ Fluorescent proteins (e.g., green fluorescent protein or mCherry) and luciferases which produce light when incubated with specific nontoxic substrates (e.g., firefly luciferase and luciferin) are commonly used for imaging bacteria in animals.⁵ Green fluorescent protein is relatively nontoxic, and variant forms have been engineered for optimal signal in bacteria.^{10,11} Mammalian tissues have significant levels of autofluorescence which interferes with the detection of fluorescent proteins, although more recent optical imagers have increased sensitivity with multispectral capabilities which can unmix fluorescent signals based on their spectral profiles.¹² Luciferases can be detected with high sensitivity due to the lack of endogenous bioluminescence in mammalian tissues, although luciferase signal can be difficult to detect in deep tissues due to optical absorption and scattering.^{13,14} Lateral image resolution of both fluorescent proteins and luciferases is highly compromised in deeper tissues

*Address all correspondence to: Roger Zemp, E-mail: rzemp@ualberta.ca

[†]These authors contributed equally in this work.

due to optical scattering, which is an intrinsic limitation of conventional optical imaging.

The lateral resolution of photoacoustic imaging, which is a hybrid optical and acoustic imaging modality, is not limited by optical scattering. Photoacoustic imaging involves irradiating a sample with a pulsed laser and light absorbed in the sample produces acoustic pressure waves, which are detected with an ultrasound transducer.^{15,16} Since acoustic scattering is far less prominent than optical scattering in tissues, photoacoustic imaging allows visualization of optical absorption with high spatial acoustic resolutions in relatively deep tissues. Chromophores with strong optical absorption produce significant photoacoustic signals. Cells expressing *lacZ*, which produces a dark-blue product in the presence X-gal, also generates strong photoacoustic signals, allowing *lacZ* to be a photoacoustic reporter gene.^{9,17} However, due to the aforementioned limitations of *lacZ*, more biologically compatible photoacoustic reporter genes would be desirable.

In mammalian cells, tyrosinase can be used as a photoacoustic reporter gene since tyrosinase is the rate-limiting enzyme involved in the production of melanin,^{18,19} which is optically absorbing and provides a strong photoacoustic signal.^{20–25} Melanin production by tyrosinase requires no exogenous substrate since the enzymatic substrate is tyrosine, an amino acid abundant in living cells. Since tyrosinase is an enzyme, one tyrosinase molecule can create multiple melanin molecules, which can amplify optical absorption and photoacoustic signal in cells. Such signal amplification is not possible for optically absorbing proteins such as chromoproteins and fluorescent proteins. When expressed in human MCF-7 breast cancer cells, tyrosinase caused cells to become visibly dark, which provided strong photoacoustic signal.²³ Several studies have validated tyrosinase as a photoacoustic reporter gene for imaging cells in animals.^{20–22,24,25} Melanin's absorption spectrum is substantially different from oxy- and deoxy-hemoglobin, allowing relatively high-resolution (<200 μm) imaging of melanin-specific photoacoustic signal with an imaging depth over 10 mm.²⁴ Such a spatial resolution at such depths cannot be achieved with traditional optical-based imaging technologies.

From our experiments, human tyrosinase does not function as a reporter gene in *Escherichia coli* cells (presumably due to membrane thickness differences between bacterial and human cells). We reasoned that bacterial tyrosinase homologues, including *mela* from *Rhizobium etli*,^{26,27} may be useful as bacterial photoacoustic reporter genes. The current study investigates the utility of *mela* as a reporter gene in *E. coli*. Since many microbiologists utilize fluorescent/luminescent reporter genes, the sensitivity and lateral resolution of photoacoustic, fluorescent, and bioluminescent imaging systems were compared by imaging *E. coli*-producing MelA or Nano-lantern, which has strong fluorescence and luciferase activity.²⁸

2 Materials and Methods

2.1 Creation of *E. coli* with Inducible Expression of Nano-lantern and *mela*

The *mela* and Nano-lantern genes were individually inserted into the pBAD/His B plasmid using standard restriction enzyme digestion and ligation reactions. Briefly, cDNAs for *mela* (kindly provided by Dr. Guillermo Gosset²⁹) and Nano-lantern (Addgene, plasmid #51970²⁸) were PCR-amplified using forward and reverse primers containing *XhoI* and *HindIII*

restriction enzyme cleavage sequences, respectively. PCR products and pBAD/His B plasmid were digested with *XhoI* and *HindIII* restriction enzymes, and reporter genes were inserted within the plasmid by ligation. Reporter gene expression was inducible through the *araBAD* promoter in the presence of L-arabinose. The pBAD/His B plasmid was modified with an A2056C mutation in the pBR322 origin, which enhanced plasmid replication at least 2-fold.

To generate the bacterial cells used for imaging, *E. coli* strain ElectroMAX™ DH10B™ (Invitrogen) was transformed by electroporation with pBAD/His B expression vectors containing *mela* or Nano-lantern. Individual bacterial colonies were used to inoculate 4 mL cultures that were grown overnight (37°C and 225 rpm) before being diluted into 50 mL of lysogeny broth (LB) medium containing 0.1 mg/mL ampicillin. These cultures were grown in 50 mL baffled shake flasks (37°C and 225 rpm) with an optical density of 0.6 to 0.7, induced with 0.02% (w/v) L-arabinose, and cultured for 48 h at 30°C before cells were collected by centrifugation. MelA-producing cultures were supplemented with 200 $\mu\text{g}/\text{mL}$ tyrosine and 20 $\mu\text{g}/\text{mL}$ copper sulfate.

2.2 Imaging *mela*-Expressing *E. coli* with Photoacoustic Imaging

In order to normalize bacterial concentrations in imaging tubes, bacteria were weighed and resuspended at specific weight to volume ratios. MelA-producing *E. coli* (1 mL) was centrifuged in preweighed tubes at 5000g for 5 min, and the supernatant was removed. Tubes with bacterial pellets were weighed again to determine bacterial weight, and bacterial pellets were resuspended at the desired concentration (mg/mL) in phosphate buffered saline (PBS). Absolute bacterial concentration (bacteria colony-forming units/mL) was determined by serially diluting bacteria at 20 mg/mL with LB medium, and dilutions were spread on plates with 100 $\mu\text{g}/\text{mL}$ ampicillin. Plates were incubated at 37°C overnight, and colonies were counted the following day.

2.2.1 Photoacoustic imaging of *mela*-expressing bacteria in water

In order to create bacterial phantoms for imaging, bacteria were resuspended at 20 mg/mL in PBS by centrifugation and were injected in perfluoroalkoxy alkane tubing (PFA, 1.06-mm inner diameter, 1.4-mm outer diameter; Scientific Commodities Inc.) using 1 mL syringes and 18 gauge needles, which sealed both ends of the tubes. Some experiments involved imaging tubes of bacteria containing serial dilutions of bacteria. Tubes containing serially diluted bacteria were immersed in water and imaged with a FujiFilm VisualSonics Vevo LAZR system using a LZ250 transducer (21 MHz) using the spectro mode with wavelengths of 680 to 970 nm with 5-nm intervals. For all photoacoustic imaging experiments, three-dimensional maximum intensity projection photoacoustic images were created using commercial Vevo software (version 1.7.2).

2.2.2 Photoacoustic imaging of *mela*-expressing bacteria between chicken tissue

To determine if *mela*-expressing cells could be imaged in tissue with optical scattering, photoacoustic imaging was performed with bacteria between chicken tissues. Briefly, 25 mL of *mela*-transformed bacterial cultures with or without *mela* induction with L-arabinose were pelleted by centrifugation. Bacterial

pellets were transferred to 200 μL thin-walled PCR tubes that were placed next to a PCR tube containing chicken embryo blood. Chicken tissue was placed between the imaging transducer and the PCR tubes to mimic tissue scattering, and tubes were imaged with the Vevo LAZR system using the spectro mode as described earlier.

2.2.3 Photoacoustic imaging of *mela*-expressing bacteria in Intralipid[®]

Photoacoustic, bioluminescent, and fluorescent imaging modalities were compared using the same phantom setup to determine the strengths and limitations of each modality. For photoacoustic imaging, two tubes of *mela*-expressing bacteria were placed side-by-side using a custom tube-holding apparatus, which positioned the tubes 10 mm from the bottom of the holder. The tubes and holder were placed in a clear plastic container that was filled with 1% Intralipid[®] solution (scattering coefficient of 1% Intralipid[®] was similar to tissue at $\sim 10\text{ cm}^{-1}$). The tubes were spaced 2, 5, 10, 15, and 20 mm apart from each other and were imaged with the Vevo LAZR system. Tubes were approximately 10-mm distance from the imaging transducer, and multispectral imaging was performed using 680, 700, 750, 800, 850, and 900 nm light. The imaging system lateral, axial, and sagittal resolutions were approximately 165, 75, and 180 μm , respectively. A stepper motor was used to translate the transducer with fixed distances, allowing reconstruction of three-dimensional images.

2.2.4 In vivo photoacoustic imaging of *mela*-expressing bacteria in the chicken embryo

To determine if *mela*-expressing bacteria can be detected inside a live animal with photoacoustics, 100 μL of *mela*-expressing bacteria were injected into the back flank of a chicken embryo, which was imaged using the Vevo LAZR system. Chicken embryos were developed as described previously, and multi-spectral imaging was performed as described earlier.³⁰ Animal work for this study was approved by the University of Alberta Animal Care and Use Committee for Livestock.

2.3 Imaging Nano-Lantern-Expressing *E. Coli* with Bioluminescence and Fluorescence Imaging

Escherichia coli-expressing Nano-lantern was resuspended in PBS at 0.5 to 10 mg/mL and added to wells of a 12-well plate with 5 $\mu\text{g}/\text{mL}$ (final concentration) coelenterazine-h added to bacteria solutions as the substrate for luciferase activity. The plate was imaged with a Bruker In-Vivo Xtreme system with back-illuminated 4 mega-pixel camera (pixel dimensions

35 \times 35 μm). Imaging was also performed with tubes as described for *mela*-expressing bacteria earlier. Nano-lantern-expressing bacteria were resuspended at 20 mg/mL, and immediately before injecting bacteria into PFA tubing (1.06-mm inner diameter, 1.4-mm outer diameter), 5 $\mu\text{g}/\text{mL}$ coelenterazine-h was added to bacteria suspensions. Tubes with bacteria had 1 mL syringes and 18 gauge needles on both ends, which sealed the tubes. Tubes were placed in a tube-holding apparatus as described earlier that was placed in a clear plastic container containing 1% Intralipid[®]. Bacteria in tubes were imaged with a Bruker In-Vivo Xtreme system using 10-s exposure for bioluminescence and 2-s exposure for fluorescence (480-nm excitation and 535-nm emission). Tubes were imaged with 5, 10, 15, and 20 mm spacing between each other with a 10-mm depth in Intralipid[®] from the bottom-facing camera.

2.4 Signal Analysis and Statistics

Photoacoustic signals from images were quantified using a MATLAB script that analyzed exported data from the Vevo LAZR system. Bioluminescence and fluorescence signals were quantified using Bruker Molecular Imaging software (v 7.1.3.20550) from the In-Vivo Xtreme system using regions of interest created on the centers of the tubes (signal from bacteria) and regions of interest created near the outer corners of the images (noise). Peak signal-to-noise ratios (PSNRs) were calculated as peak signal from bacteria/standard deviation of noise. To determine the minimum number of *mela*-expressing bacteria that can be detected with the Vevo LAZR system, the concentration of bacteria was multiplied by the voxel volume ($9.33 \times 10^{-6}\text{ cm}^3$) that was divided by the PSNR from the photoacoustic images. For comparing photoacoustic/fluorescence/bioluminescence imaging modalities for resolving bacteria in optically scattering medium, intensity plots from tubes were acquired in ImageJ using the rectangle selection tool, which was at least twenty pixels along the tubes. Full-width at half-maximum values were acquired from intensity plots using the fwhm MATLAB function available at MATLAB Central.³¹

3 Results and Discussion

3.1 Photoacoustic Imaging of Phantoms Containing *E. Coli* Expressing *mela*

In the absence of induced *mela* expression with L-arabinose, *E. coli* transformed with pBAD/His B plasmid containing *mela* had a normal light yellow color. *Escherichia coli* cultured with L-arabinose induced *mela* expression, which caused the

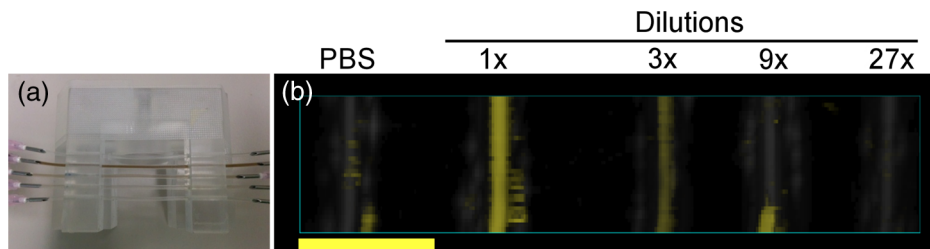


Fig. 1 Photoacoustic imaging of *Escherichia coli*-expressing *mela*. (a) Imaging setup of tubes containing phosphate buffered saline (PBS) with or without serially diluted bacteria expressing *mela*. (b) Top-down view of the three-dimensional photoacoustic image of tubes shown in (a). Photoacoustic and ultrasound signals are shown in yellow and gray scale, respectively. Scale bar represents 5-mm distance.

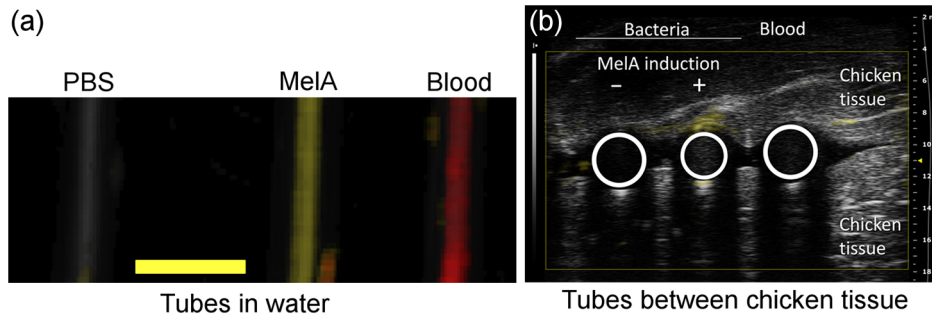


Fig. 2 Photoacoustic imaging of blood and *E. coli*-expressing *mela*. (a) Tubes containing PBS, *mela*-expressing bacteria (20 mg/mL), and chicken embryo blood were imaged with photoacoustics at multiple wavelengths. Shown is a top-down view of the three-dimensional image of the tubes. *mela* and oxy-hemoglobin-specific photoacoustic signals were unmixed with Vevo software and are shown in yellow and red, respectively, over a gray scale ultrasound image. Scale bar represents 3-mm distance. (b) Bacterial pellets with or without *mela* induction as well as chicken embryo blood were imaged in 200 μ L tubes under approximately 10 mm of chicken tissue. Tube positions are marked by the white circles.

bacteria to become dark [Fig. 1(a)], with much of the produced melanin secreted into the growth medium since the medium was still dark after centrifugation of bacteria. The effect of *mela* on bacteria proliferation was assessed by enumerating colonies from bacterial cultures with or without *mela* induction. Induction of *mela* in *E. coli* had no effect on proliferation during the exponential growth phase when bacteria reached a near-maximum concentration at 6-h culture (data not shown). After bacteria concentration plateaued, *mela* expression caused fewer colony-forming units in culture compared to bacteria without *mela* induction. This delayed toxicity may be due to the high expression levels caused by the *araBAD* promoter. A previous study by Jathoul et al.²⁰ demonstrated that tyrosinase expression in 10 different human cell lines had minimal effect on cell growth, suggesting that tyrosinase enzymes such as *mela* may have minimal cell toxicity when expressed at moderate levels.

The sensitivity of imaging *mela*-expressing bacteria with photoacoustics was determined by imaging tubes containing 1-, 3-, 9-, and 27-fold serial dilutions of *mela*-expressing bacteria, which corresponded to approximately 9×10^8 , 3×10^8 , 1×10^8 , and 3.3×10^7 bacteria/mL, respectively. Tubes with bacteria were submerged into a water bath and imaged with the Vevo LAZR system using the 21 MHz LZ250 transducer. Photoacoustic signal was observed along some regions of the tube containing PBS that likely corresponded to air bubbles and/or low levels of signal from the top of the plastic tube. Due to this background signal, the only photoacoustic signals analyzed were those within the tubes. Photoacoustic signal was detected in tubes with up to 9-fold diluted bacteria solutions with a PSNR of 55 [Fig. 1(b)]. Given that the 9-fold diluted sample had approximately 1×10^8 bacteria/mL, the estimated minimum number of bacteria detectable with our system was ~ 20 bacteria/voxel. The estimated minimum number of bacteria detectable with our photoacoustic system (and all photoacoustic systems) will depend on a variety of factors including the concentration of bacteria and the physical volume of the bacterial sample that will affect the frequency of emitted photoacoustic waves.

To determine if the photoacoustic signal from *mela* can be separated from that of blood using multispectral unmixing, imaging experiments were performed with tubes containing blood, PBS, or *mela*-expressing *E. coli* in PBS. The photoacoustic

spectrum of *mela*-expressing bacteria was similar to that of melanin, which allowed spectral unmixing of the *mela* signal from that of blood [Fig. 2(a)]. All tubes contained at least a few regions with photoacoustic signals corresponding to *mela* or blood suggesting that the unmixing algorithm within the Vevo software was not perfect. However, the vast majority of photoacoustic signal classification was appropriate for blood and *mela*-expressing bacteria. To determine if *mela*-expressing bacteria can be visualized in an environment with optical scattering similar to tissue, *mela*-expressing bacteria were pelleted in 200 μ L PCR tubes, placed underneath ~ 10 mm of chicken tissue, and imaged with the Vevo LAZR system. When imaged underneath chicken tissue, the *mela*-specific photoacoustic signal was detectable from *mela*-expressing bacteria [Fig. 2(b)]. Very little *mela*-specific photoacoustic signal was detectable from bacteria without *mela* induction [Fig. 2(b)]. Surprisingly, the photoacoustic signal was not detectable from the tube containing chicken embryo blood. The 10 mm of chicken tissue may have absorbed/scattered much of the lower wavelengths of light that blood preferentially absorbs. Compared to blood, *mela* produced relatively greater levels of photoacoustic signal at longer wavelengths which can penetrate tissue with higher efficiency, possibly explaining the greater photoacoustic signal from the tube of *mela*-expressing bacteria compared to the tube of blood.

3.2 Comparing Fluorescence/Bioluminescence/Photoacoustic Imaging with *E. Coli* Expressing Nano-Lantern or *mela*

To illustrate the imaging resolution disadvantages of fluorescence and bioluminescence imaging in an optical scattering medium, we created *E. coli* transformed with pBAD/His B plasmid containing Nano-lantern, which is a very bright chimera of a yellow fluorescent protein and *Renilla* luciferase.²⁸ To verify that bacteria expressing Nano-lantern produce fluorescence and bioluminescence, bacteria expressing Nano-lantern were diluted at 0.5 to 10 mg/mL in a 12-well plate and imaged with a Bruker In-Vivo Xtreme system (Fig. 3). In the absence of an optically scattering medium, fluorescence and bioluminescence signals from bacteria were very strong with PSNR > 400 at 10 mg/mL bacteria. Although 0.5 mg/mL bacteria expressing Nano-lantern provided relatively little fluorescence and

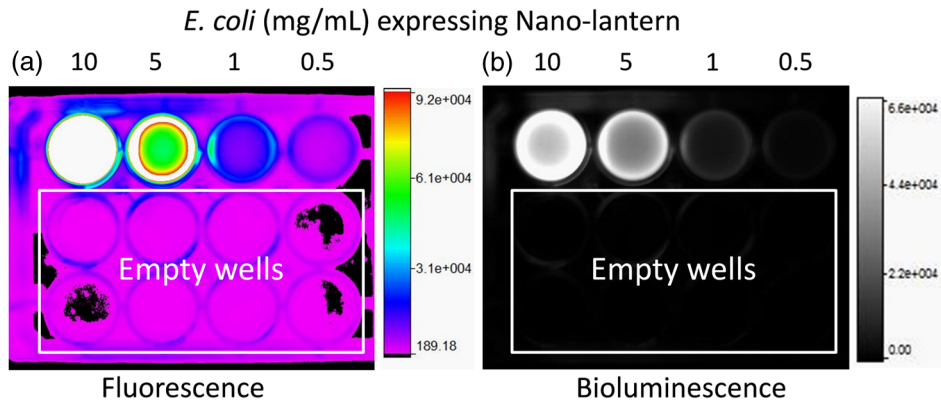


Fig. 3 (a) Fluorescence and (b) bioluminescence imaging of *E. coli*-expressing Nano-lantern. Bacteria were diluted at different concentrations, aliquoted into wells of a 12-well plate, and imaged with a Bruker In-Vivo Xtreme system. Only the first row of wells contained bacteria.

bioluminescence signals, longer exposure times for fluorescence and bioluminescence imaging would theoretically increase the PSNR for these dilutions, allowing smaller amounts of bacteria to be detected. The results suggest that in the absence of an optically scattering medium, bacteria expressing Nano-lantern can be imaged with greater sensitivity with bioluminescence and fluorescence imaging compared to bacteria expressing *melA* imaged with photoacoustics.

However, when two tubes containing bacteria expressing Nano-lantern were spaced between 5 and 20 mm apart at a depth of 10 mm in 1% Intralipid® (to mimic optical scattering in tissue), the fluorescence and bioluminescence signals from the two tubes significantly overlapped even when tubes were separated by 15 mm (Fig. 4). The two tubes could only be visually resolved when they were separated by 20 mm which is nearly 20-fold the inner diameter of the tubes. A similar

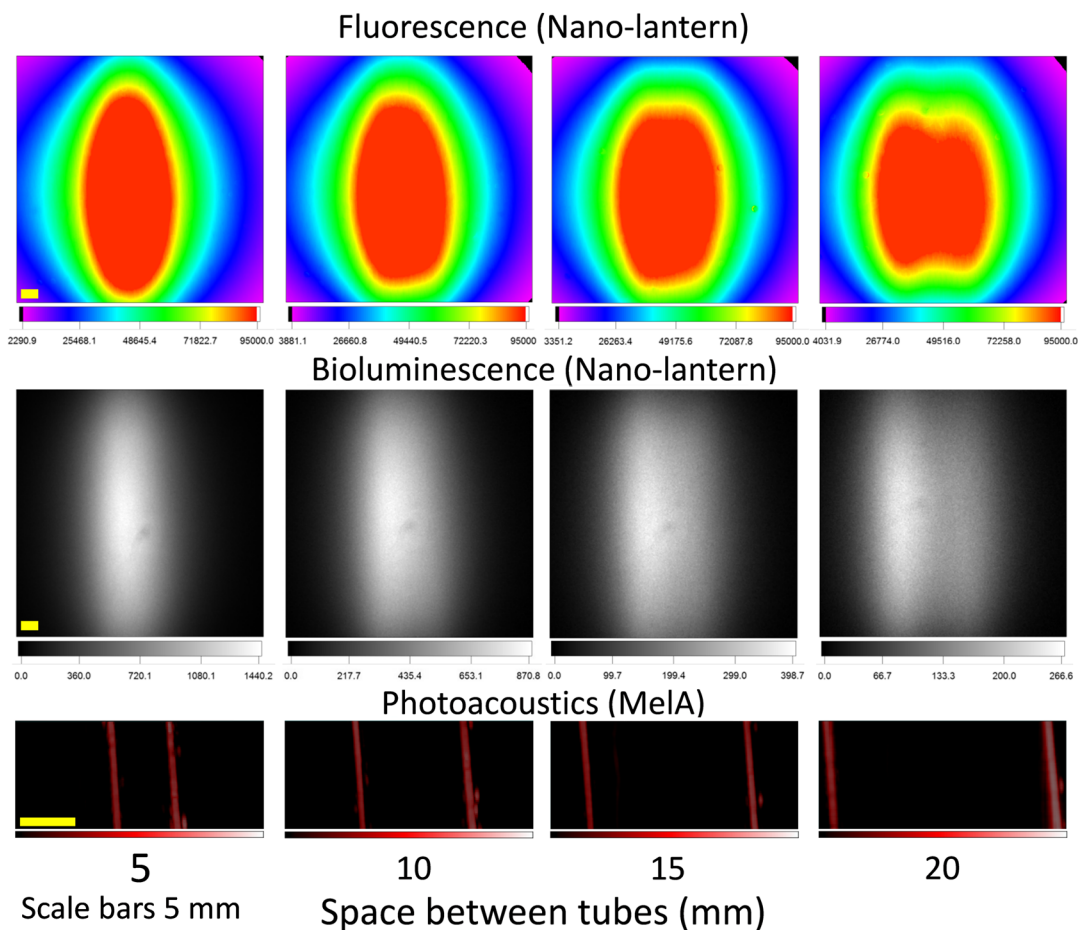


Fig. 4 Comparison of Nano-lantern and *melA* as reporter genes for fluorescence/bioluminescence and photoacoustic imaging, respectively. Two tubes of bacteria expressing Nano-lantern or *melA* were spaced between 5 and 20 mm from each other and were imaged as indicated. Tubes were submerged 10-mm deep in 1% Intralipid® to mimic tissue optical scattering. Scale bars correspond to 5-mm lengths.

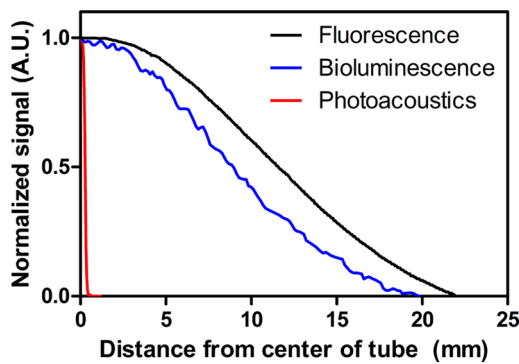


Fig. 5 Intensity plots of images of single tubes containing *melA* or Nano-lantern-expressing bacteria, which were submerged 10-mm deep in 1% Intralipid[®] and imaged with photoacoustics or fluorescence/bioluminescence, respectively.

experiment was performed but using tubes containing bacteria expressing *melA*, which were submerged 10 mm in 1% Intralipid[®] and imaged using photoacoustics. The tubes could be resolved even when the tubes were less than 1 mm from each other (data not shown). Intensity plots from individual bacteria-containing tubes provided full-width at half-maximum values of 26.5, 19.5, and 0.499 mm when tubes were imaged with fluorescence, bioluminescence, and photoacoustics, respectively (Fig. 5), demonstrating the advantage of photoacoustics over fluorescence and bioluminescence for imaging in optically scattering environments at relatively high depths (~10 mm).

3.3 *In Vivo* Photoacoustic Imaging of *melA*-Expressing *E. Coli* Injected in a Chicken Embryo

Although chicken tissue has significant optical scattering, it lacks much of the blood normally found in healthy tissue, which can influence local fluence levels and background photoacoustic signal. To determine the *in vivo* utility of *melA* as a bacterial reporter gene for photoacoustic imaging, experiments with live animals are required. The chicken embryo model was used due to the model's relative ease-of-use, rapid growth, and low cost.^{30,32–34} *melA*-expressing bacteria (approximately 100 μ L of 20 mg/mL *E. coli*) was injected in the back flank

of a chicken embryo, and the injection site was imaged with photoacoustics. *melA*-specific photoacoustic signal was detected at the bolus injection site that was unmixed from that of oxy- and deoxy-hemoglobin, all of which were laid over an ultrasound image detailing the anatomical structures within the embryo (Fig. 6). Some photoacoustic signal corresponding to *melA* can be seen outside the injection site, which may be due to embryo movement during imaging with different laser wavelengths that can cause signal misclassification. The presence of bubbles in the ultrasound coupling gel typically generated a *melA* signal below the bubble in the embryo as seen on the right side of Fig. 6. *melA*-specific signal could be detected almost 20-mm deep into tissue with a lateral resolution less than 200 μ m. As demonstrated in Fig. 4, such resolution at that depth is not achievable with fluorescence and bioluminescence due to optical scattering, which limits the resolution of purely optical imaging modalities.

Although it is relatively easy to compare resolution differences between photoacoustic, fluorescence, and bioluminescence imaging, it is more complicated to compare sensitivity differences between these imaging modalities. Optical scattering of fluorescent and bioluminescent signals complicates the reconstruction of the signals in three dimensions. As such, fluorescent and bioluminescent signals generated from Nano-lantern-expressing cells created two-dimensional images with signal intensities that cannot be directly compared to the photoacoustic signals from the three-dimensional images of *melA*-expressing bacteria. Additionally, the sensitivity of optical imaging modalities is dependent on exposure time, which further complicates comparisons of detection sensitivity of bacteria expressing *melA* and Nano-lantern. Longer exposure times provide greater sensitivity for optical imaging but may be impractical, especially due to the time-dependent depletion of luciferase substrate needed for bioluminescence. Based on our results, fluorescence and bioluminescence imaging can provide very high sensitivity for detecting bacteria expressing Nano-lantern when the bacteria are near the CCD camera with minimal optical scattering between the bacteria and camera. At these superficial depths, *melA*-expressing bacteria will also allow high-resolution photoacoustic images with the lateral resolution dependent on the ultrasound transducer frequency. Photoacoustic image sensitivity is greatest when imaging at superficial depths since laser fluence is highest at the tissue

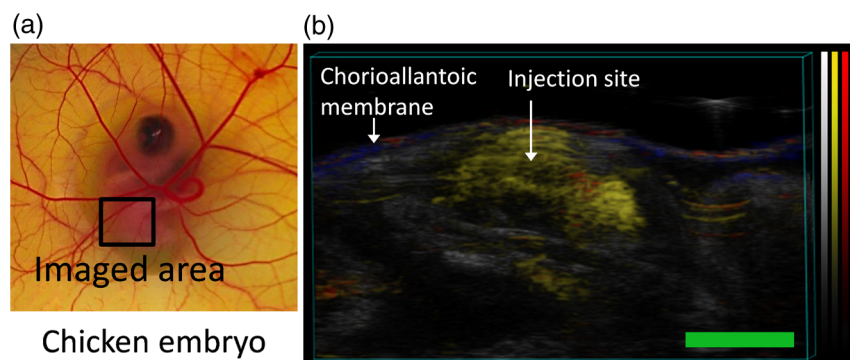


Fig. 6 *In vivo* photoacoustic imaging of *melA*-expressing bacteria. (a) Representative image of a chicken embryo, which was the model used for *in vivo* imaging. (b) Multispectral three-dimensional photoacoustic and ultrasound image of a 100 μ L bolus injection of *melA*-expressing bacteria in the back flank of a chicken embryo. Yellow, red, and blue represent the *melA*, oxy-hemoglobin, and deoxy-hemoglobin photoacoustic signal, respectively. Ultrasound is shown in gray scale. Green scale bar represents 5-mm distance.

surface where there is minimal laser energy loss due to light scattering. As imaging depth increases, photoacoustic signal will decrease with decreasing laser fluence although resolution remains relatively unaffected due to low acoustic scattering in tissue. For high-resolution images of bacteria found relatively deep in tissue, *mela* may be a more appropriate reporter gene to be visualized with photoacoustics.

For *in vivo* experiments, melanin secreted from *mela*-expressing cells will provide a photoacoustic signal thus, in order to determine the location of cells, *mela* expression should be induced relatively soon before imaging. Alternatively, the continuous secretion of melanin from bacteria may be useful to track the migration paths of bacteria in animals using photoacoustic imaging.

mela is a tyrosinase homologue and as such requires oxygen for activity. Most common fluorescent proteins (e.g., green fluorescent protein and mCherry) and luciferases also require oxygen, thus anaerobic bacteria will require other reporter genes such as flavin binding proteins and SNAP-f fluorescent proteins to track gene expression and/or visualize anaerobic bacteria.^{35–39}

The current study demonstrates that *mela* can be used as a photoacoustic reporter gene for imaging *E. coli*. Expression of *mela* in *E. coli* causes significant melanin production causing the bacteria to become highly optically absorbing, which causes the bacteria to provide high contrast in photoacoustic imaging. When imaging in optically scattering environments (e.g., tissue), *mela* provides superior spatial resolution compared to fluorescent and luciferase reporter genes, since resolution in photoacoustic imaging is not affected by optical scattering. Future studies should involve tracking pathogenic bacteria with *mela* for precise assessment of the locations of infectious colonies in animals. Whole-animal tomographic photoacoustic imaging systems could be used to allow visualization of bacteria throughout entire animals.⁴⁰ Such experiments would allow noninvasive visualization of infection processes of pathogenic bacteria in entire live animals at unprecedented resolutions.

Acknowledgments

We gratefully acknowledge funding from Natural Sciences and Engineering Research Council of Canada (355544-2008, 375340-2009, 288338-2010 to R.E.C., STPGP 396444), Canadian Institutes of Health Research (MOP-123514 to R.E.C.), Terry-Fox Foundation and the Canadian Cancer Society (TFF 019237, TFF 019240, CCS 2011-700718, 702032 to both R.Z. and R.E.C.), the Alberta Cancer Research Institute (ACB 23728), the Canada Foundation for Innovation, Leaders Opportunity Fund (18472), Alberta Advanced Education and Technology, Small Equipment Grants Program (URSI09007SEG), Microsystems Technology Research Initiative (MSTRI RES0003166), University of Alberta Startup Funds, Alberta Ingenuity/Alberta Innovates scholarships for graduate and undergraduate students, Canadian Federation of University Women Edmonton Margaret Brine Graduate Scholarships for Women, and SPIE Optics and Photonics Education Scholarship. Dr. Lewis holds the Frank and Carla Sojonyk Chair in Prostate Cancer Research supported by the Alberta Cancer Foundation.

References

1. A. A. Gilad et al., "MRI reporter genes," *J. Nucl. Med.* **49**(12), 1905–1908 (2008).
2. T. Jiang, B. Xing, and J. Rao, "Recent developments of biological reporter technology for detecting gene expression," *Biotechnol. Genet. Eng. Rev.* **25**, 41–75 (2008).
3. J. J. Min and S. S. Gambhir, "Molecular imaging of PET reporter gene expression," *Handb. Exp. Pharmacol.* **185** (Pt 2), 277–303 (2008).
4. H. Youn and J. K. Chung, "Reporter gene imaging," *AJR Am. J. Roentgenol.* **201**(2), W206–W214 (2013).
5. F. X. Campbell-Valois and P. J. Sansonetti, "Tracking bacterial pathogens with genetically-encoded reporters," *FEBS Lett.* **588**(15), 2428–2436 (2014).
6. M. C. Lane et al., "Expression of flagella is coincident with uropathogenic *Escherichia coli* ascension to the upper urinary tract," *Proc. Natl. Acad. Sci. U. S. A.* **104**(42), 16669–16674 (2007).
7. J. S. Wright, III, R. Jin, and R. P. Novick, "Transient interference with staphylococcal quorum sensing blocks abscess formation," *Proc. Natl. Acad. Sci. U. S. A.* **102**(5), 1691–1696 (2005).
8. T. J. Silhavy and J. R. Beckwith, "Uses of lac fusions for the study of biological problems," *Microbiol. Rev.* **49**(4), 398–418 (1985).
9. L. Li et al., "Photoacoustic imaging of lacZ gene expression in vivo," *J. Biomed. Opt.* **12**(2), 020504 (2007).
10. B. P. Cormack, R. H. Valdivia, and S. Falkow, "FACS-optimized mutants of the green fluorescent protein (GFP)," *Gene* **173**(1 Spec. No.), 33–38 (1996).
11. J. D. Pedelacq et al., "Engineering and characterization of a superfolder green fluorescent protein," *Nat. Biotechnol.* **24**(1), 79–88 (2006).
12. L. Zhou and W. S. El-Deiry, "Multispectral fluorescence imaging," *J. Nucl. Med.* **50**(10), 1563–1566 (2009).
13. L. F. Greer, III and A. A. Szalay, "Imaging of light emission from the expression of luciferases in living cells and organisms: a review," *Luminescence* **17**(1), 43–74 (2002).
14. E. D. Jansen et al., "Effect of optical tissue clearing on spatial resolution and sensitivity of bioluminescence imaging," *J. Biomed. Opt.* **11**(4), 041119 (2006).
15. C. Li and L. V. Wang, "Photoacoustic tomography and sensing in biomedicine," *Phys. Med. Biol.* **54**(19), R59–R97 (2009).
16. L. V. Wang and S. Hu, "Photoacoustic tomography: in vivo imaging from organelles to organs," *Science* **335**(6075), 1458–1462 (2012).
17. L. Li et al., "Simultaneous imaging of a lacZ-marked tumor and microvasculature morphology in vivo by dual-wavelength photoacoustic microscopy," *J. Innovative Opt. Health Sci.* **1**(2), 207–215 (2008).
18. W. S. Oetting, "The tyrosinase gene and oculocutaneous albinism type 1 (OCA1): a model for understanding the molecular biology of melanin formation," *Pigm. Cell Res.* **13**(5), 320–325 (2000).
19. P. A. Riley, "Melanin," *Int. J. Biochem. Cell Biol.* **29**(11), 1235–1239 (1997).
20. A. P. Jathoul et al., "Deep in vivo photoacoustic imaging of mammalian tissues using a tyrosinase-based genetic reporter," *Nat. Photonics* **9**, 239–246 (2015).
21. A. Krumholz et al., "Photoacoustic microscopy of tyrosinase reporter gene in vivo," *J. Biomed. Opt.* **16**(8), 080503 (2011).
22. Y. Laufer et al., "In vivo photoacoustic imaging of tyrosinase expressing tumours in mice," *Proc. SPIE* **8223**, 82230M (2012).
23. R. J. Paproski et al., "Tyrosinase as a dual reporter gene for both photoacoustic and magnetic resonance imaging," *Biomed. Opt. Express* **2**(4), 771–780 (2011).
24. R. J. Paproski et al., "Multi-wavelength photoacoustic imaging of inducible tyrosinase reporter gene expression in xenograft tumors," *Sci. Rep.* **4**, 5329 (2014).
25. C. Qin et al., "Tyrosinase as a multifunctional reporter gene for photoacoustic/MRI/PET triple modality molecular imaging," *Sci. Rep.* **3**, 1490 (2013).
26. M. I. Chavez-Bejar et al., "Metabolic engineering of *Escherichia coli* to optimize melanin synthesis from glucose," *Microb. Cell Fact.* **12**, 108 (2013).
27. S. Pinero et al., "Tyrosinase from *Rhizobium etli* is involved in nodulation efficiency and symbiosis-associated stress resistance," *J. Mol. Microbiol. Biotechnol.* **13**(1–3), 35–44 (2007).
28. K. Saito et al., "Luminescent proteins for high-speed single-cell and whole-body imaging," *Nat. Commun.* **3**, 1262 (2012).
29. N. Cabrera-Valladares et al., "Expression of the *mela* gene from *Rhizobium etli* CFN42 in *Escherichia coli* and characterization of the encoded tyrosinase," *Enzyme Microb. Technol.* **38**(6), 772–779 (2006).

30. C. F. Cho et al., "Evaluation of nanoparticle uptake in tumors in real time using intravital imaging," *J. Vis. Exp.* (52) 2808 (2011).
31. P. Egan, "FWHM: to calculate the full-width at half-maximum of an input," 2006, <http://www.mathworks.com/matlabcentral/fileexchange/10590-fwhm> (27 July 2015).
32. K. H. Kain et al., "The chick embryo as an expanding experimental model for cancer and cardiovascular research," *Dev. Dyn.* **243**(2), 216–228 (2014).
33. H. S. Leong et al., "Intravital imaging of embryonic and tumor neovasculation using viral nanoparticles," *Nat. Protoc.* **5**(8), 1406–1417 (2010).
34. T. D. Palmer et al., "Integrin-free tetraspanin CD151 can inhibit tumor cell motility upon clustering and is a clinical indicator of prostate cancer progression," *Cancer Res.* **74**(1), 173–187 (2014).
35. S. Chapman et al., "The photoreversible fluorescent protein iLOV outperforms GFP as a reporter of plant virus infection," *Proc. Natl. Acad. Sci. U. S. A.* **105**(50), 20038–20043 (2008).
36. T. Drepper et al., "Reporter proteins for in vivo fluorescence without oxygen," *Nat. Biotechnol.* **25**(4), 443–445 (2007).
37. A. Mukherjee et al., "Characterization of flavin-based fluorescent proteins: an emerging class of fluorescent reporters," *PLoS One* **8**(5), e64753 (2013).
38. O. Nicolle et al., "Development of SNAP-tag-mediated live cell labeling as an alternative to GFP in *Porphyromonas gingivalis*," *FEMS Immunol. Med. Microbiol.* **59**(3), 357–363 (2010).
39. J. Potzkei et al., "Real-time determination of intracellular oxygen in bacteria using a genetically encoded FRET-based biosensor," *BMC Biol.* **10**, 28 (2012).
40. R. Ma et al., "Multispectral photoacoustic tomography (MSOT) scanner for whole-body small animal imaging," *Opt. Express* **17**(24), 21414–21426 (2009).

Robert J. Paproski is a research associate in the Departments of Oncology and Electrical and Computer Engineering at the University of Alberta, Edmonton, Canada. His research focuses on novel applications of ultrasound in oncology, photoacoustic reporter gene development, as well as automated image and data analysis.

Robert E. Campbell is a professor of chemistry of the University of Alberta, Edmonton, Canada. His research is focused on the development of improved fluorescent proteins and new fluorescent protein-based reporters for biological research. His contributions have been recognized with a number of awards, including the 2015 Rutherford Memorial Medal in Chemistry from the Royal Society of Canada. Fluorescent protein-based tools developed in his lab have been requested more than 3300 times.

Biographies for the authors are not available.